CONF-73-121-E
FERMILAB-CONF-73-121-E 14A

P-P Inelastic Scattering at Small Momentum Transfer * †

Juliet Lee-Franzini
State University of New York, Stony Brook, New York 11790

ABSTRACT

A series of experiments on proton-proton inelastic scattering were performed at NAL and ISR. The four-momentum transfer in these experiments ranges from .01 to 1.75 $(GeV/c)^2$ and the equivalent laboratory momentum ranges from 50 to 2,000 (GeV/c). The results clearly show the existence of two components. For one of these the cross section $d^2\sigma/dtdM_X^2$ scales as 1/s. For small M_X^2 a second component is present. Its cross section is independent of energy and is bounded by $3.2 < \sigma_{diff} < 4.7$ mb.

The subject of my talk is "p-p inelastic scattering" at small momentum transfer". This seemingly restrictive title actually allows me to discuss a good portion of proton inclusive cross section. This is because the inelastic cross section constitutes about 80% of the total cross section, and a momentum transfer interval of about 0.2 $(GeV/c)^2$ at small t includes approximately 70% of that inelastic cross section. Therefore, understanding what happens in p-p inelastic scattering at small momentum transfer gives one knowledge on over half of the p-p inclusive reactions. 80% of σ_T

The major questions considered in this paper are 1) what we have learned experimentally in this region at high energy accelerators such as NAL and ISR, and 2) what kind of data is forthcoming in the coming year from these accelerators. Only the general features of the lower energy experiments will be discussed, and mainly as a background introduction, since they have all been covered extensively at past conferences.

Before starting, let us define some kinematical quantities. Consider the reaction

$$p_1 + p_2 \rightarrow p_{obs} + X \qquad (1)$$

where at ISR the two protons are coming at each other, and at NAL one proton is the beam proton, the other proton is stationary. We call the observed proton p_{obs}, and at NAL it is the recoil proton. In ISR experiments it is the particle moving in the general direction of p_1 with transverse momentum p_T and longitudinal momentum p_ℓ times x, where x is the Feynman variable $(2p_L^*/\sqrt{s})$. We give the name X to the quasi particle which is comprised of all the other reaction products with momentum p_i, $i = \alpha,\beta...N$. Clearly

$$p_X^4 = p_1^4 + p_2^4 - p_{obs}^4.$$

* Supported in part by the National Science Foundation.
† Invited talk at the Fifth International Conference on High Energy Collisions, Stony Brook, August, 1973.

We can define two Lorentz invariant parameters

1. (a) $t = (p_{obs} - p_{target})_\mu \, (p_{obs} - p_{target})_\mu$

and is $\simeq -p_T^2$ near $x = 1$, $t = \dfrac{-p_T{}^2 - M_p^2 (1 - x)^2}{x}$ at ISR

(b) $t = -2\, m_p\, T$ where T is the kinetic energy of the recoil proton, at NAL.

2. (a) $M_X^2 = (\Sigma\, p_i)_\mu \, (\Sigma\, p_i)_\mu = (p_1 + p_2 - p_{obs})_\mu \, (p_1 + p_2 - p_{obs})_\mu$

It is often called the effective mass squared and is approximately related to the Feynman variable by

(b) $\dfrac{M_X^2 - M_{proton}^2}{s} = 1 - x$ where s is the total center of mass energy squared, i.e., $s = (p_1 + p_2)^2$.

For completeness we can add $u = (p_1 - p_{obs})^2$, where of course $s + t + u = M_X^2 + 3\, m_p^2$.

Having defined these quantities let us turn to the general features of $p + p \to p + X$ at BNL-PS[1] energies.

1) The mass spectrum of X at lower energies tended to be full of peaks and valleys, corresponding to the well known resonances, in fact some of them were discovered that way. With increasing energy it became more smooth.

2) This recoil distribution is known to be generally rapidly falling with increasing momentum transfer. Typically, it was measured to be of the form $e^{-b|t|}$ where b lies between 5 and 20 $(GeV/c)^2$

3) There is an energy independent component for this inelastic scattering cross section.

4) The target recoil distribution is characteristic of diffraction from an object of the size of about one Fermi.

Good and Walker[2], well before these facts were known, had pointed out a coherent inelastic scattering mechanism which would give an energy independent contribution to σ_{in} and called it "diffraction dissociation". To observe it a very simple geometric condition has to be satisfied. This is essentially the requirement of coherence across the depth of the target.

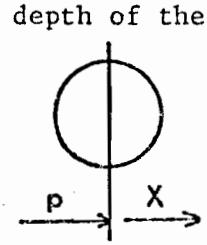

$\Delta\lambda < r$

$\Delta p \Delta x = \hbar = 1$

$\Delta p = \dfrac{1}{\Delta x} \approx \dfrac{1}{r}$

In terms of the masses of p and X, and the incident momentum, this condition can be written as

$$\Delta p = \frac{M_X^2 - M_p^2}{2\, p_{lab}} < \frac{1}{r} \simeq M_\pi$$

or

$$M_X^2 < 2\, p_{lab}\, M_\pi$$

so for 30 GeV $\quad M_X^2 < 2 \times 30 \times \frac{1}{7} \simeq 9\ \mathrm{GeV}^2$

at 300 GeV $\quad M_X^2 < \frac{2 \times 300}{7} \simeq 90\ \mathrm{GeV}^2$

Therefore one could expect large masses to be produced diffractively at NAL and ISR energies, and it was believed by some that this process could become an increasingly dominant part of the inelastic scattering cross section.[3] In Regge language this "diffraction dissociation" portion of the cross section is often interpreted as arising from the exchange of a Pomeron.[4] Using the Mueller approach one can further describe this region in terms of "triple Regge couplings".[5]

We would like to know the composition of the inelastic cross section, and perhaps from prime principles explain them. From an inclusive experiment, what physical information can one obtain? First of all, the M_X^2 spectrum, which might look something like this:[6]

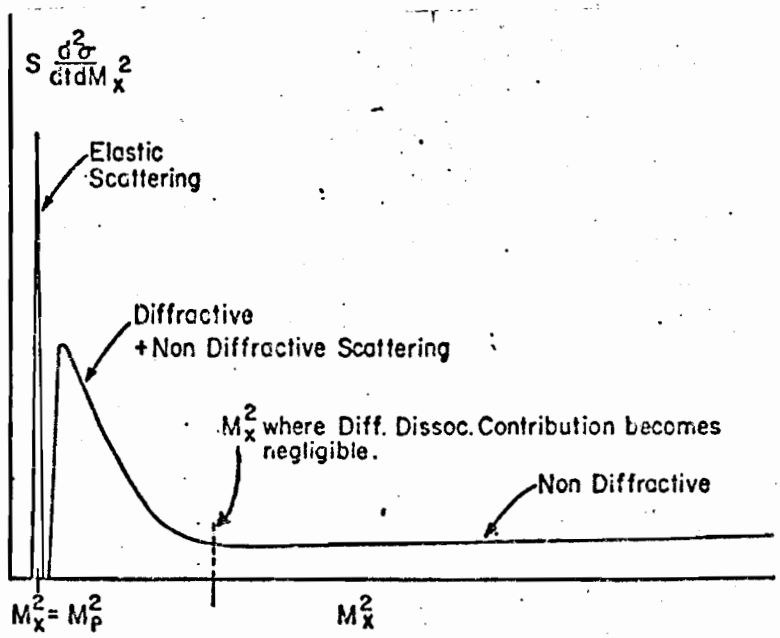

Figure 1. $s \frac{d^2\sigma}{dt dM_X^2}$ versus M_X^2, not to scale.

For each M_X^2 region one could measure its s dependence, its t dependence, and of course its cross section. Not all experiments can measure every one of these quantities, and each measures each variable over a limited range. In discussing the data gathered by each experiment, one must keep this in mind. Some experiments, such as the bubble chamber experiments, can in principle measure all these quantities, but are hampered by serious lack of statistics. Without too much complication one could also measure the multiplicity associated with each M_X^2 region, and two of the experiments to be discussed have done this in a preliminary way.

Let us now consider how such experiments are carried out experimentally. Consider Equation (1) where, at ISR, one is in the center of mass system and each proton (p_1, p_2) has an energy of $\sqrt{s}/2$ about 30 GeV. Since $\langle p_T \rangle_{ave} \simeq .3$ GeV, one must have a resolution of better than approximately $\frac{.3}{30} \simeq 1\%$ to measure the features of the cross section. The scattering angle is typically of the order of 8 milliradians, or half a degree; hence one needs to get to very small angles with respect to the p_1 or p_2 direction. The ISR experiments which I am reporting on are confined to a minumum angle of about 20 mr (both the single arm spectrometer of CHLM[7] and double arm spectrometer of ACHGT[8]), hence do not reach the low t region. Most of the data is of $t \simeq -.3$ and above. Note also that since the ISR beams have a spread of about 2%, even using refinements such as reconstructing the interaction point in the crossing region to determine the orbital radii of the interacting protons, one can only reduce the 2% spread to about 0.7%. Hence one obtains a rather broad resolution of the order of 9 GeV^2 in the CHLM experiment, and the order of 25 GeV^2 in the case of the ACHGT collaboration.

On the other hand, it is ten times harder to measure the forward proton's deviation at NAL energies. For example, let us take the same $\Delta p \simeq .3$ GeV, and consider a proton at lab momentum of 300 GeV. Then,

$$\frac{\Delta p}{p} \simeq \frac{.3}{300} \simeq 0.1\% \quad \approx 1\,\text{mrad}$$

$.05^\circ \quad \frac{1}{50^\circ/\text{mrad}} = \frac{5\times10^{-2}}{50} = 1\,\text{mrad}$

and the $1/2^\circ$ scattering becomes .05 degrees, quite hard to measure. Therefore, all experiments at NAL choose to look at the slow recoil proton, and ignore the proton which plows ahead more or less in the same direction as the beam proton. To appreciate the advantage of observing the recoil proton, we recall that in this case $t = -2M_pT$ where T is the kinetic energy of the proton, and a $|t|$ of $\simeq 0.2$ corresponds to a proton of about 100 MeV, and that if one were to look at all protons of kinetic energy from, say, 0 energy to 100 MeV, and assuming a t dependence of e^{-bt} ($b \approx 6$)

$$\int_{-.2}^{0} \frac{dN}{dt}\, dt \Big/ \int_{-\infty}^{0} \frac{dN}{dt}\, dt = 70\% \qquad (2)$$

It does, however, require different techniques to study these 100

MeV protons, and we will come back to that.

As for the angle, the recoil proton now comes out in a range near 90° in the laboratory, and the $\Delta\theta$ is greatly magnified. Let us take elastic scattering as a guide, zero momentum transfer corresponds to 90° in the laboratory, and approximately

$$\frac{\pi}{2} - \theta \simeq \sqrt{\frac{T_{proton}}{2M_{proton}}} \simeq \sqrt{\frac{0.1}{2}} \simeq 13^o$$

for a 100 MeV elastically scattered proton. Recoils from inelastically scattered events, in the same T range, appear at $\theta < 90^o$, depending on the value of M_X. Approximately (to 10% accuracy) we have

$$\cos\theta \simeq \frac{M_X^2 - M_p^2 + 2\, p_{beam} T}{2\, p_{beam}\ 2\, M_p T}$$

Therefore, in general the lower the T, the closer to 90° one measures, the lower the M_X^2 one is sensitive to. To illustrate, let us consider two extreme examples at NAL: the U.S.-Soviet Union[9] collaboration is located in the 90° region and measures protons up to 14 MeV, they see $M_X^2 \simeq 2$; the Rutgers-Imperial College[10] collaboration looked at recoils around 60°, with $T > 70$ MeV, most of their data are at large M_X^2 ($X < .91$) in the larger t region ($|t| > .15$).

The bubble chamber experiments at NAL also look at the recoil proton, but I will say very few words about them since Jack Van de Velde is summarizing their contribution for this conference. The main point is that they scan for dark, short tracks which would indicate the presence of a low energy proton, measure its angle to the beam direction, its length to obtain from range its energy, and thereby deduce t and M_X^2. By counting the number of tracks associated with the proton in the same event, they also obtain the multiplicity distribution. The solid angle is clearly good, nearly 4π; energy determination is good, but the angle measurement of a short track is not too well determined, and the number of events per exposure is normally of the order of about a few thousand per energy.[11]

I shall now discuss each of the five counter experiments which measure inelastic scattering.

A. The CHLM*Collaboration-Small Angle Spectrometer.

The earliest result on proton inelastic scattering was from the CHLM group at the ISR, in fact almost all the data from this group has been published.[7] They use a single arm spectrometer with two septum magnets inserted into the ISR ring to intercept a 40% momentum interval, and a 16 m radian angular interval. There are three magnets to do the momentum analysis, three Cerenkov counters to separate different particles, and wire spark chambers at the entrance and exits of the magnets and Cerenkov counters. Scintillation counters are placed along the particle path to give a trigger

* CHLM (CERN, Holland, Lancaster, Manchester)

when a particle goes through the system. Other counters are placed before the crossing region to monitor luminosity and background. The first two Cerenkov counters and the two septum magnets are mounted on supports which allow for displacements and rotation in the vertical plane. The total accessible angular range is from 25-200 m rad.

The events are reconstructed off line by computing the momentum and angle of production from the spark coordinates and the bending power of the magnets.

$\Delta p \simeq \pm 1\%$ and $\Delta\theta \simeq 2$ m rad

The data I will show have

$8 < p_{proton} < 15.3$ GeV/c and 35 mr $< \theta < 100$ mr.

In order to get those events whose x is very near 1, i.e., $M_X^2 \Rightarrow 0$, they added a small five element hodoscope M, installed at the side of the intersection opposite the Small Angle Spectrometer. Near x = 1, the events are a mixture of elastically scattered and inelastically produced protons. They are separated by :

1) Particle in spectrometer is extrapolated to the crossing region in order to determine the orbital radii of the interacting protons.
2) Using the point of interaction and the momentum compaction function of the ISR at the crossing point, one reduces Δp by a factor of 3 from the Δp of 2% at the ISR.
3) Events with momenta near the beam momenta (mainly elastically scattered events) have a peak in the auxilliary hodoscopes central counter (M_3).
4) Hence one obtains the inelastic events by requiring an anticoincidence with this center counter during analysis, and adding a momentum dependent correction for the residual inelastic content of M_3.

The results of these experiments can be summarized by looking at Figures 2-4. In Figure 2 one sees the elastic proton spectrum and the inelastic proton spectrum near x = 1. The elastic peak has a full width at half maximum of 150 MeV/c, corresponding to a mass resolution of $\Delta M_X^2 \simeq 9$ GeV^2.

In Figure 3, the inelastic proton spectra are shown for various p_T^2 values. Note that there is a broad "basin" at x = .8 - .9, which seems to move toward x = 1 with increasing p_T^2. The CHLM group have measured the invariant $\frac{Ed^3\sigma}{dp^3}$ at several s. The general features of the data are similar; for x < .8, scaling is good to 10%.

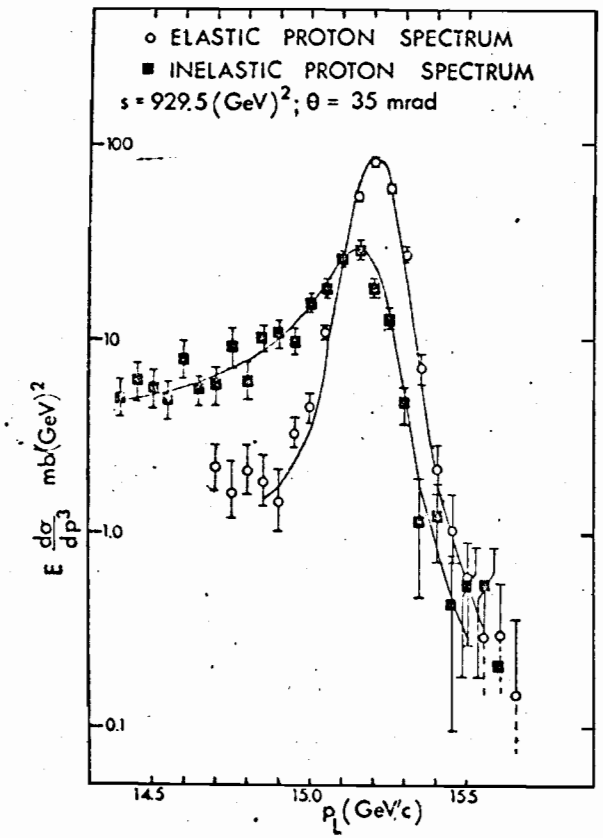

Figure 2. $E \frac{d\sigma}{dp^3}$ mb/(GeV)^2 versus p_L(GeV/c) for Elastic Proton Spectrum and for Inelastic Proton Spectrum.

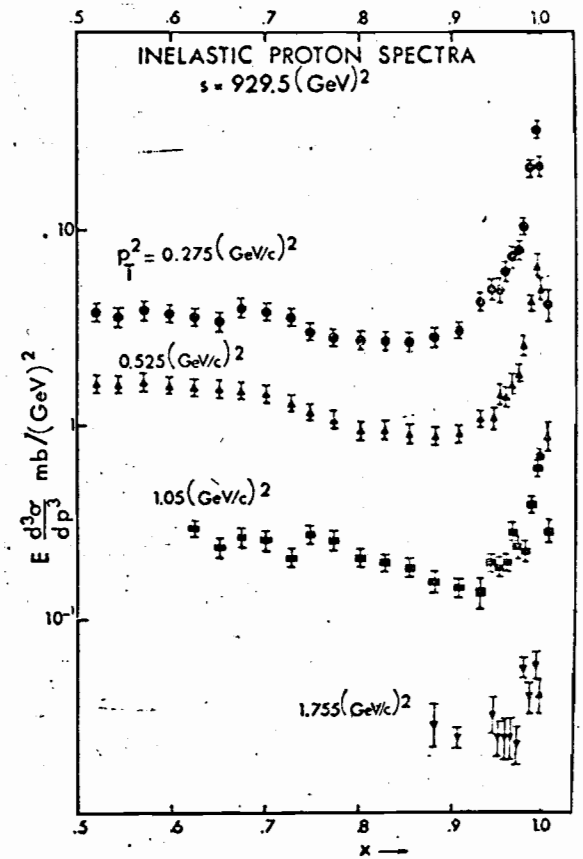

Figure 3. $E \frac{d^3\sigma}{dp^3}$ mb/(GeV)^2 versus x for Inelastic Proton Spectra.

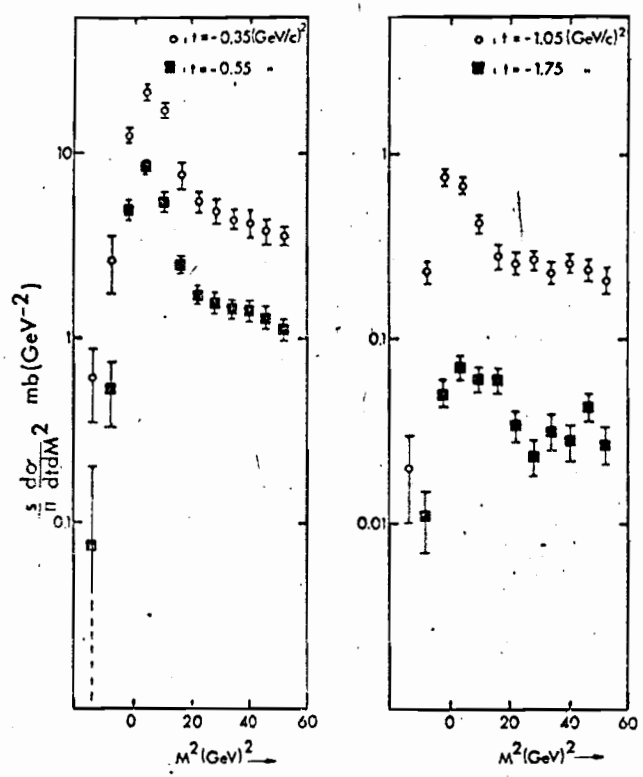

Figure 4. $\frac{s}{\pi}\frac{d^2\sigma}{dtdM_X^2}$ versus M_X^2 $(GeV)^2$ at s = 929.5 GeV^2

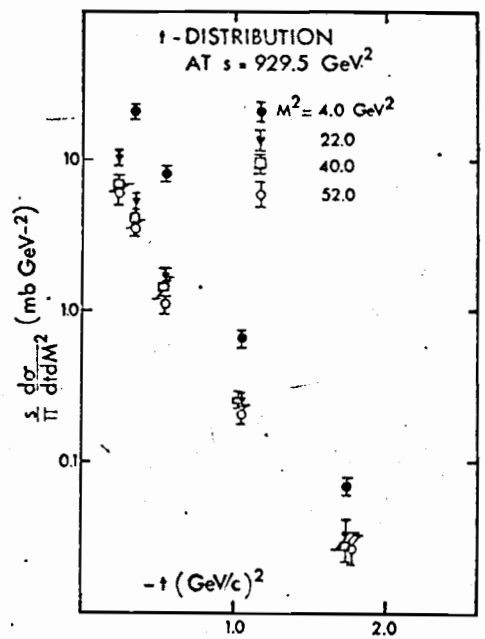

Figure 5. $\frac{s}{\pi}\frac{d\sigma}{dtdM_X^2}$ versus $-t(GeV/c)^2$ at s = 929.5 GeV^2

In Figure 4 is plotted the doubly differential cross section $\frac{s}{\pi}\frac{d^2\sigma}{dtdM_X^2}$ versus the Missing Mass M_X^2. The four curves ranging in $t = -.35$ to $t = -1.75$ show a gradual broadening of the forward peak. In short, the peak sharpens as $|t|$ decreases.

In Figure 5 the same doubly differential cross section is plotted versus t for various M_X^2. One notes that they can not be fitted by straight lines, hence the t dependence can not be fitted by a single exponential.

The CHLM group has also measured the multiplicity for $x > .99$ $\langle n\rangle = 2.8 \pm 0.5$ and for $.72 < x < .84$ $\langle n\rangle = 6.7 \pm 1.5$.[12]

B. The ACHGT* Collaboration- Double Arm Spectrometer

This experiment has not been published yet. All information reported here on the experiment and the analysis had been given to me by Professor G. Goldhaber, who was spending a sabbatical leave at CERN working on this experiment. There is a double arm spectrometer, one arm above the beam on one side, the other below the beam on the other side. They are at fixed angle, each subtending a θ interval of 70 mr (from 20 to 90 mr), ϕ interval of 2 radians. There is only one magnet, in contrast to the three of CHLM, and the momentum resolution is about 2.5%.

There are in addition, two sets of auxiliary jet counters, each in four pieces which subtend an angle from 160 to 400 m rad. The normal event is triggered by a coincidence of two counters, two in each arm, which signify one particle has gone through one arm in coincidence with a particle going through the other arm.

With the auxiliary counters they can further tag whether several particles have gone in coincidence, opposite to the one particle in one arm. These are called "single jet" events. These can be further classified as those which had 1-2 extra particles (medium multiplicity), and those which had 3-4 extra particles (high multiplicity). When both sets of auxiliary counters fired, the event is referred to as a "double jet" event. One studies the 2 tracks which went through the system, and locates its position on an $e|x_1|$, $e|x_2|$ plot where $e = \pm 1$ corresponds to the charge of the particle, and x is the usual Feynman variable.

The interesting thing is the correlation between the type of event and its population in the $e|x_1|$, $e|x_2|$ plot. The elastic events appear as a blob in the upper right hand corner. The double jet events are in the center of the plot. The "single jet" events cluster in a dark band along the edge decreasing towards the center. Finally, when the requirement of single jet plus low multiplicity is imposed, and one is left with the two edge bands, which corresponds to "diffractively dissociated events". Figure 6 shows the aforementioned situations.

* ACHGT (Aachen, CERN, Harvard, Genova, Torino)

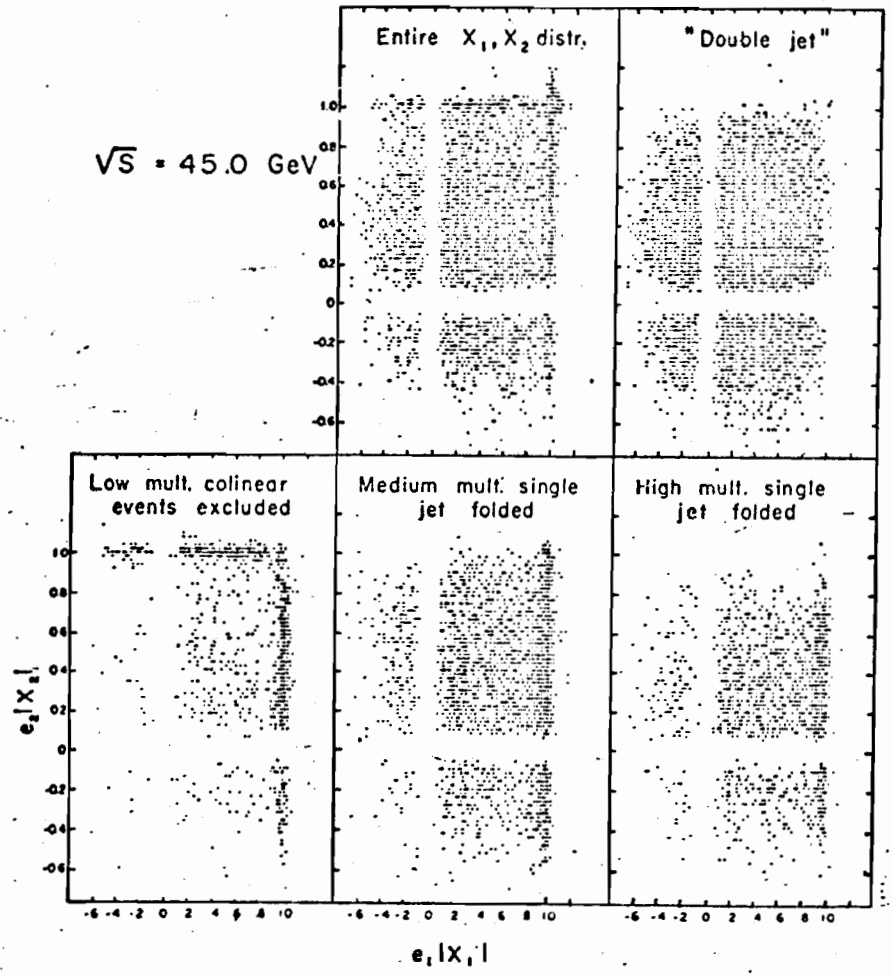

Figure 6. $e_2|x_2|$ versus $e_1|x_1|$ for various event types.

M_X^2 distributions are shown in Figure 7. The major features are 1) the peak of the M_X^2 distribution seem to shift toward larger values as the associated multiplicity is larger, 2) the tail in the M_X^2 distribution gets higher and higher as the multiplicity increases; this is interpreted by G. Goldhaber to mean that larger M_X^2's are produced from diffraction dissociation.

In this experiment normalization has not been done yet, so one does not obtain an absolute cross section. At different values of s, different values of t are sampled, and these are plotted on one graph in Figure 8. Here, too, one sees that a single exponential could not fit all four curves, i.e., the effective slope is continuously changing.

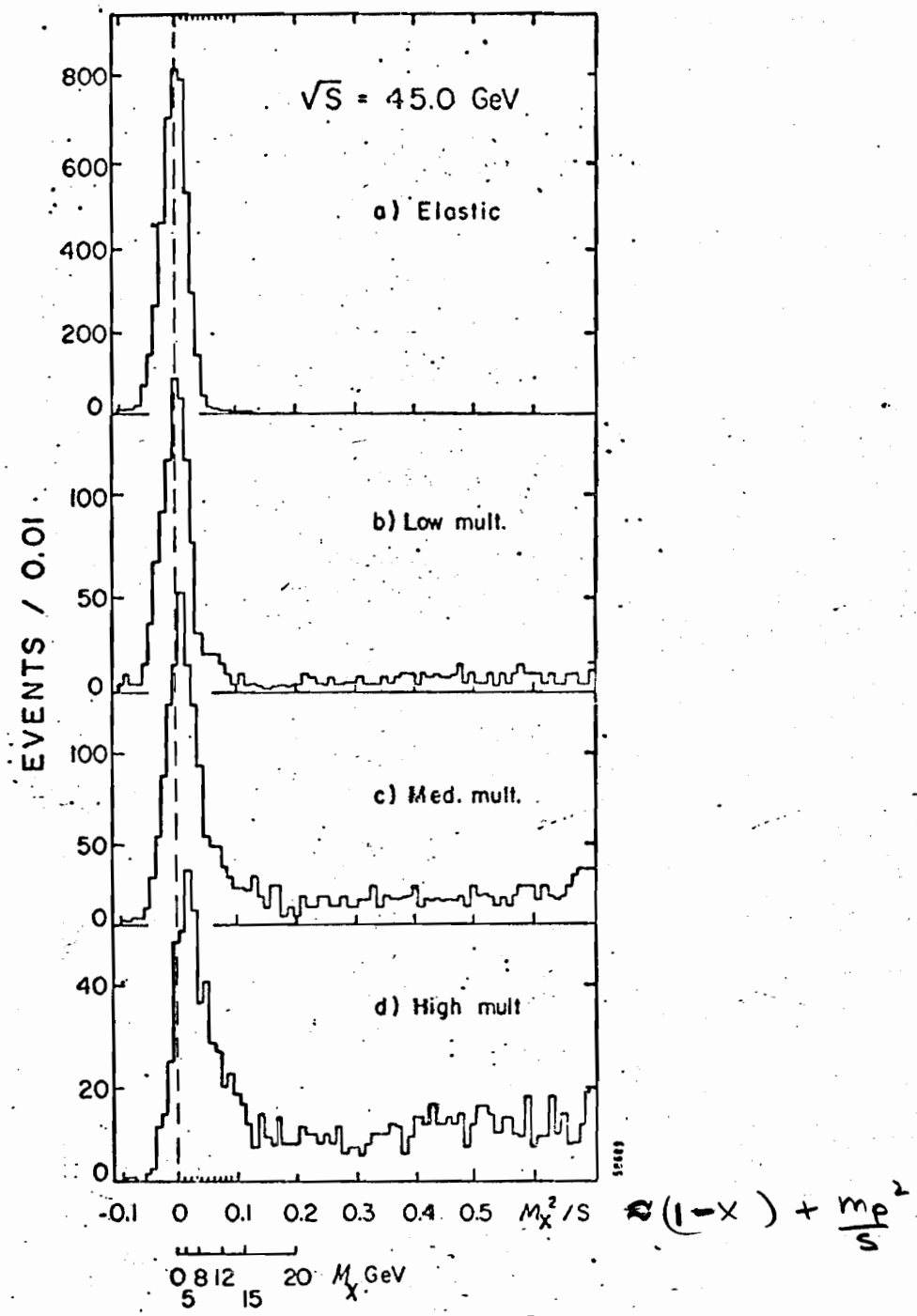

Figure 7. Events/0.01 versus M_X^2/s

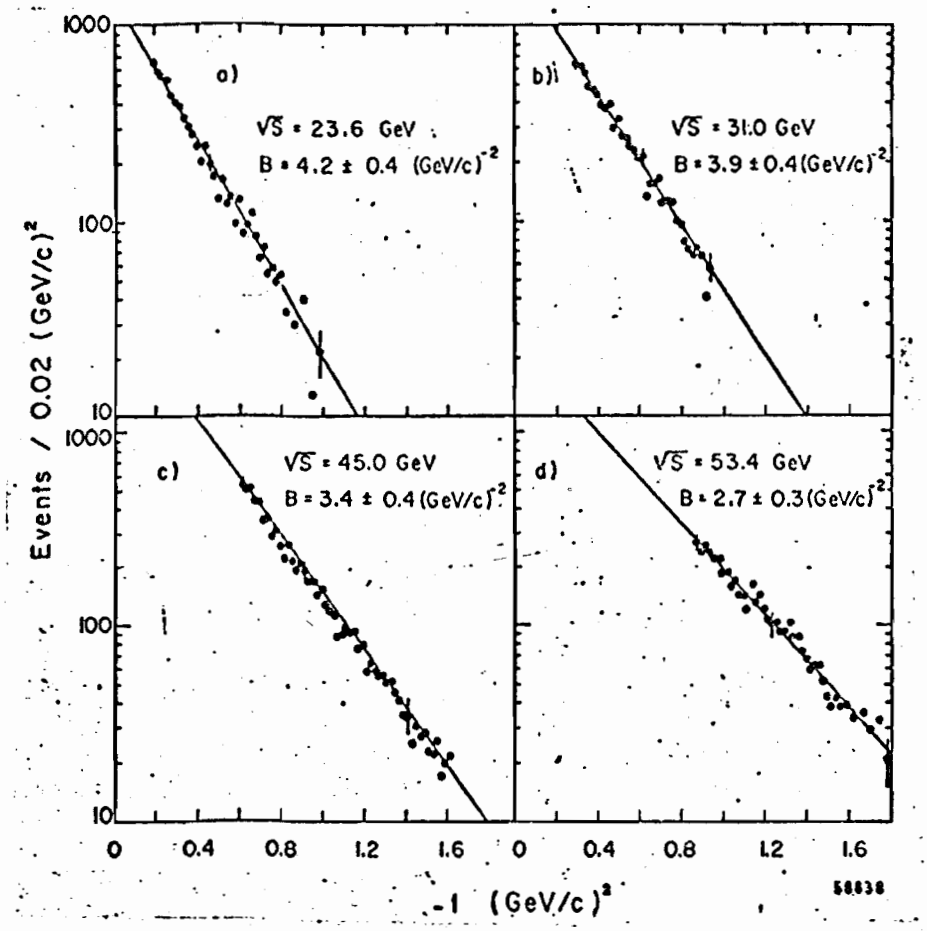

Figure 8. $\frac{dN}{dt}$ (Arbitrary Units) versus $-t(\mathrm{GeV/c})^2$

C. Rutgers-Imperial College Collaboration.[10] (Sannes et al)

They study $p + p \rightarrow p + X$ in the region $108 < s < 752$ GeV^2, $0.14 < |t| < 0.38$ GeV^2 and $.80 < x < .93$. The data were taken during the accelerator ramp (50 to 400 GeV) of the National Accelerator, using the internal H_2 jet target facility. The recoil protons which were emitted between 55° and 65°, with β between .34 and .57, pass through a scintillation counter telescope and stop in a total absorption scintillation counter. The recoil momentum is determined by time of flight. Pulse height in the absorption counter was used to remove pion contamination. The accuracy in measuring s, t and x are $\Delta s=30$ GeV^2, $\Delta t=0.05$ GeV^2 and $\Delta x=0.01$.

A solid state detector, located at 85.5°, monitored the rate of the elastically scattered protons at $t=-.22$ GeV/c)^2. To the extent that the σ total and σ elastic remain in constant ratio, monitoring the elastically scattered proton is monitoring luminosity of the beam-jet crossing. Corrections for the change in total over the s range (+8%) and elastic slope parameter (-3%) were made. Using the known elastic cross section dσ/dt and other normalization, $s\,\frac{d^2\sigma}{dt\,dM_X^2}$ was obtained

Data at five s values and four t values are plotted as a function of x in Figure 9. In their kinematic region, $0.14 < |t| < 0.38$ GeV^2, can be described by a simple exponential e^{bt} (see Figure 10), where b is not a function of s and depends only very weakly on x.

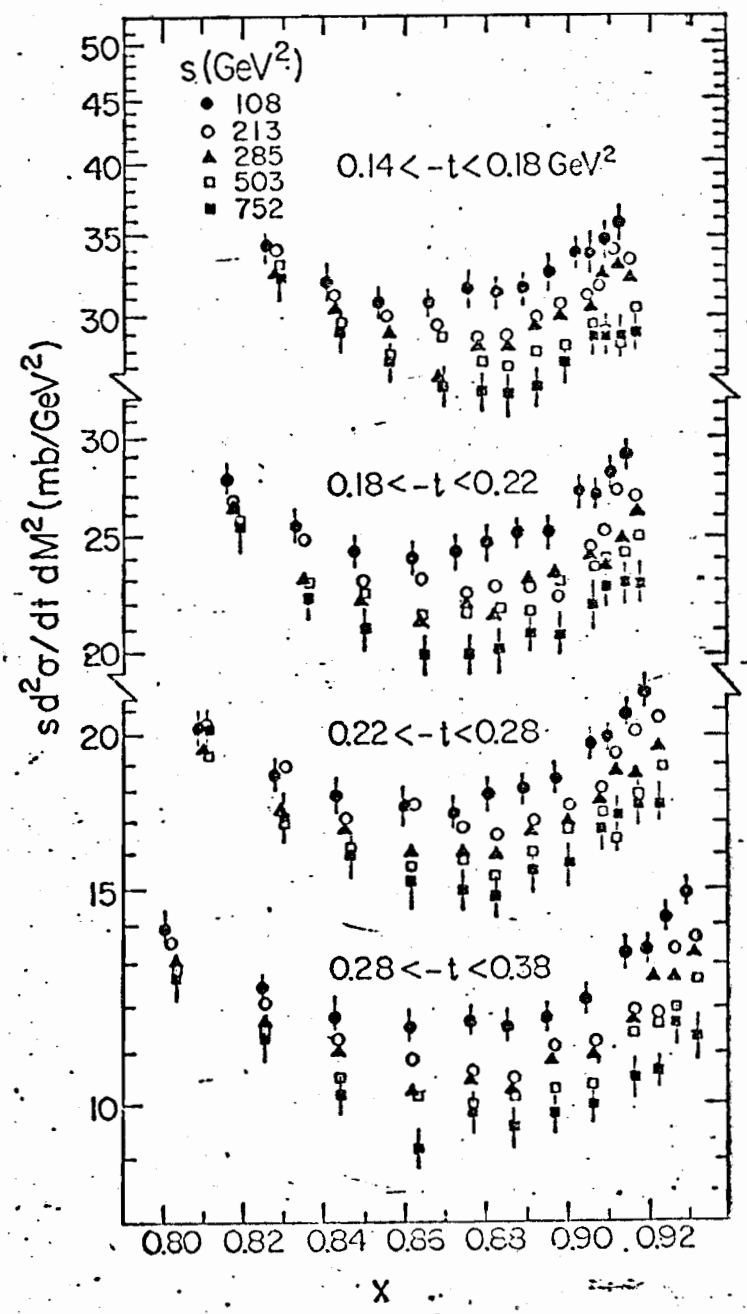

Figure 9. $sd^2\sigma/dtdM_X^2(mb/GeV^2)$ versus x

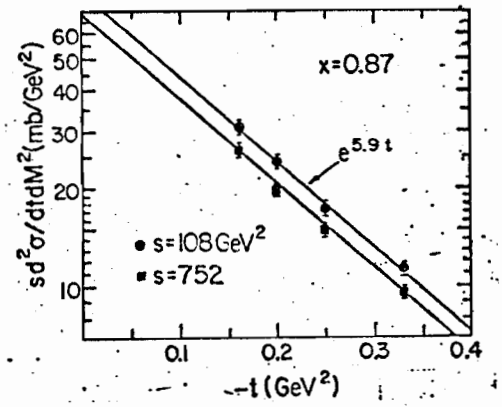

Figure 10. $sd^2\sigma/dtdM_X^2(mb/GeV^2)$ versus $-t(GeV^2)$

Fits of the form

$$sd^2\sigma/dtdM_X^2 = A(x)\ e^{b(x)t}\ \left|1 + B(x)s^{-1/2}\right|. \qquad (3)$$

to their data at fixed x and t show almost no variation of the parameter B with t. They therefore make an overall fit of the form (3) to their data at all values of s and t, and arrive at the parameters given in the following table.

$x = 1-M_X^2/s$	A (mb/GeV^2)	B(GeV)	$b(GeV^{-2})$
0.83	71 ± 7	1.9 ± 0.7	5.9 ± 0.3
0.85	64 6	2.5 0.7	5.9 0.3
0.87	61 5	3.0 0.6	5.9 0.3
0.89	62 4	3.6 0.5	6.0 0.3
0.91	66 3	4.3 0.4	6.1 0.3

The dip in the x-distributions of Figure 9 near x = 0.88 is reflected in the A parameters of the above table, which also have a minimum near x = 0.88. The b parameter, within errors, is constant with x, while the B parameter increases significantly with x, indicating a relatively stronger s-dependence at large x. The s-dependence of their data is shown in Figure 11, in which the invariant cross section at x = 0.83 and 0.91 is plotted versus $s^{-1/2}$.

I have some reservations regarding the validity of this experiment's results, especially at small s. In Figure 12 the data of Figure 9 is replotted in terms of M_X^2. The disturbing aspect is that the "dip" seems to follow the center of their M_X^2 spectrum interval, and at s = 108 no forward diffractive peak is seen at small masses, and a rise is noted at masses of about 20 GeV^2.

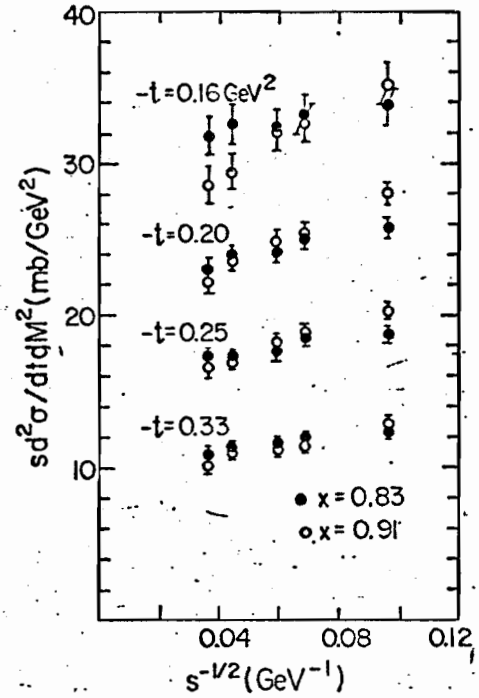

Figure 11. $sd^2\sigma/dtdM_X^2$ versus $s^{-1/2}(GeV^{-1})$

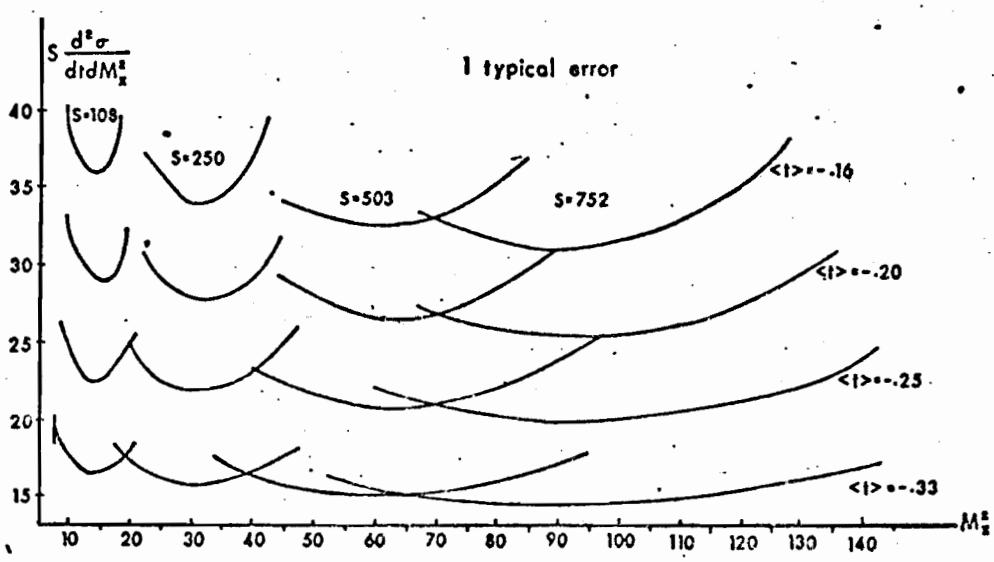

Figure 12. $sd^2\sigma/dtdM_X{}^2$ versus M_X^2

D. U.S.-U.S.S.R. Collaboration[9] (Rochester, Rockefeller, Dubna)

This experiment is performed at the Internal Target Area of the National Accelerator Laboratory. The target is a hydrogen gas jet. The experiment's primary purpose was to study small $|t|$ p-p elastic scattering, therefore, the detectors are located very close to 90° to the beam direction and are sensitive to lower energy recoil protons. Solid state detectors were used to measure the recoil proton's kinetic energy, but only for the case of stopping protons corresponding to a maximum kinetic energy of 14 MeV. Note that a 14 MeV elastically scattered proton would emerge at about 85° and its momentum transfer $|t| = -2M_pT$ is .028 (GeV/c). Therefore, this group is particularly suited to investigate low t and small M_X^2 in elastically scattered events. In looking at the results from this group one should bear in mind the close interweaving of the M_X^2 and t, so that unlike other groups which present M_X^2 spectra for different constant t, here for each M_X^2 spectrum several $|t|$ values are involved and are so indicated (Figure 13 and Figure 14).

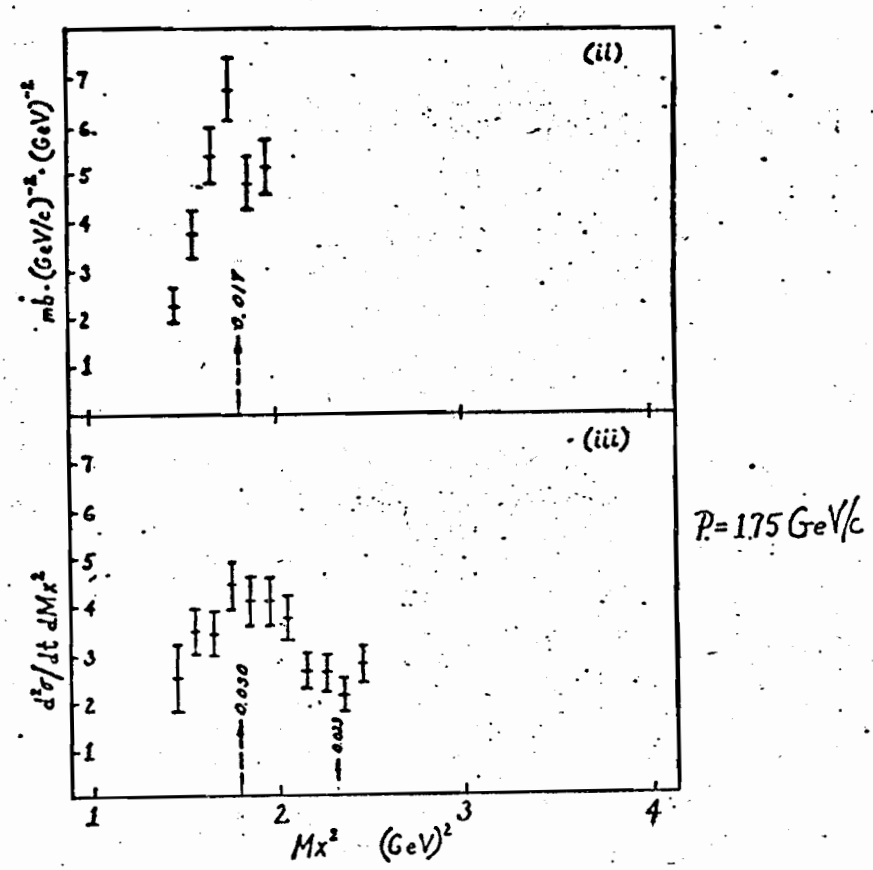

Figure 13. $d^2\sigma/dtdM_X^2$ mb · $(GeV/c)^{-2}$ · $(GeV)^{-2}$ versus M_X^2 $(GeV)^2$ at P_{in} = 175 GeV/c

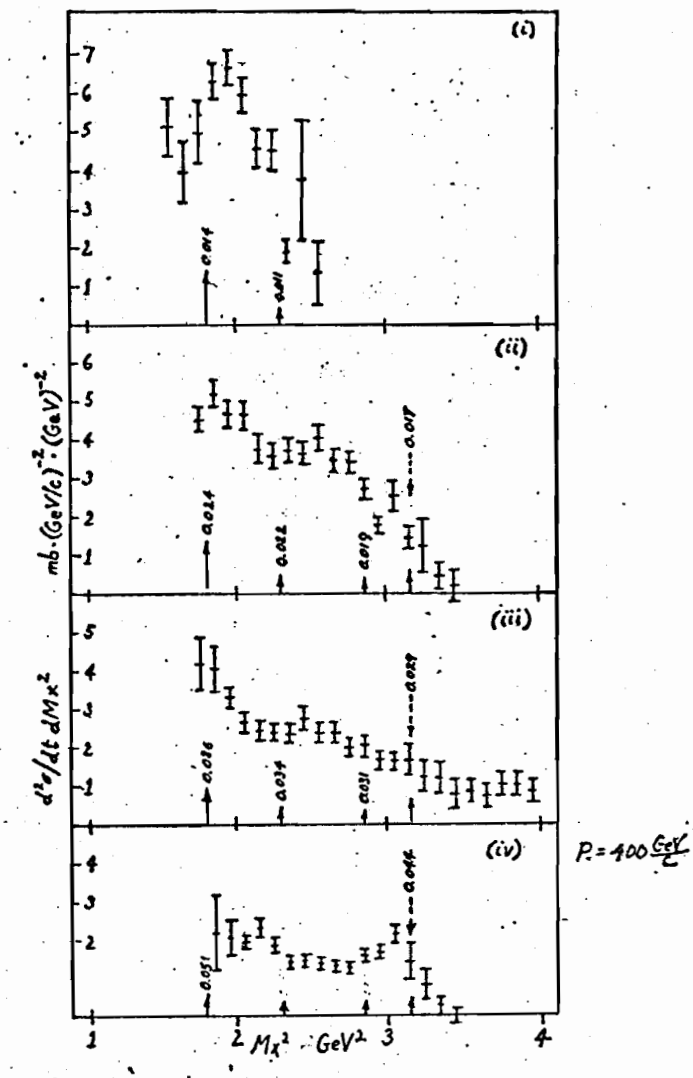

Figure 14. $d^2\sigma/dtdM_X^2$ mb · $(GeV/c)^{-2}$ · $(GeV)^{-2}$ versus M_X^2 GeV^2 at P_{in} = 400 GeV/c

This data was presented by Professor R. Cool at the Berkeley Conference and has not yet appeared in published form. In Figure 13 we see such a mass spectra taken at an incident momentum of 175 GeV/c. One notes the sharp onset of the inelastic cross sections peaking at M_X^2 of 1.8 for $|t|$ = .017, and the peak has decreased in magnitude at t = .030. In Figure 14 the incident momentum was 400 GeV/c. One notes again the peak at $M_X^2 \simeq 2$ at $|t| \simeq .013$ $(GeV/c)^2$ and it decreases in magnitude as $|t|$ increases. This led to a determination of the slope b in an e^{-bt} dependence for this peak of b ≃ 15. This peak is most likely the $N^*(1400)$. The differential cross section and the slope for the production of this N^* has the same value as measured at AGS-PS energies.[1]

E. CFL-FMS* Collaboration[13]: Columbia Stony Brook.

This experiment was performed at NAL, using the extracted proton beam in the Neutrino Laboratory. Data were first obtained at 200 GeV/c incident beam momentum. The detailed description of the apparatus, data analysis procedure, as well as results from that run have been published in the Vanderbilt conference proceedings.[14] The present discussion concentrates on the results of a 300 GeV/c run which is still under analysis, hence is preliminary.

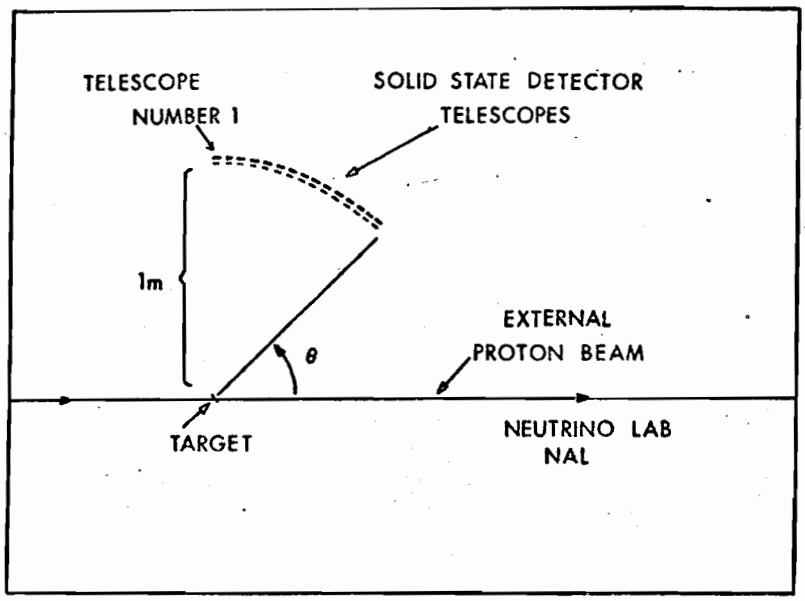

Figure 15. Schematic of solid state detector hodoscope in NAL Neutrino Lab beam line.

We measure the kinetic energy T of the recoil proton and its angle θ with a solid state detector hodoscope consisting of 18 telescopes forming an arc of one meter radius from the beam-target interaction point, spanning a θ interval from 89° to 48°. See Figure 15. For target, instead of gas or liquid hydrogen we chose to use polyethylene and carbon foils (6.5 mg/cm^2, ≈ 5 mm wide placed at 45° to the beam) and perform a subtraction. The range of T measured is between 10 and 100 MeV, corresponding to $|t|$'s between .019 and .19. Each telescope subtends an angular opening of .4°. Therefore only 20% of the above-mentioned angular span is sampled for a given target position. To decrease the effect of such gaps we took data from four target positions, differing slightly in the coordinate of the target along the beam direction. The M_X^2 range measured was from 0 to 100 GeV^2.

The first detector in each telescope pair is 500 μ thick, and

* CFL-FMS (Childress, Franzini, Lee-Franzini, McCarthy, Schamberger, the five experimenters).

the second is 5000 μ. The two detectors together give a dE/dx - E measurement and thus allow particle identification as well as T determination. This experiment involved extensive and ingenious electronics design[15] to overcome the very short effective spill length in the extracted proton beam prior to July 1973. One example of the electronics design is the use of hardware for initial data reduction which allowed each event to be processed in 17 μsec, enabling us to accept up to 4000 events/machine pulse.[16] The data I am going to discuss was collected in eight hours.

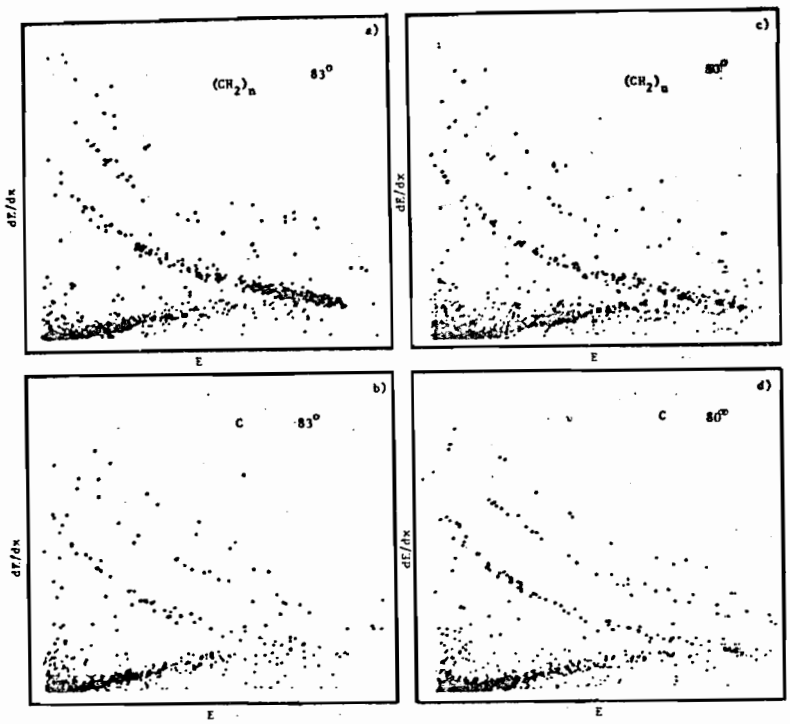

Figure 16. dE/dx-E plots for (a) polyethylene data at 83° (b) carbon data at 83° (c) polyethylene data at 80° (d) carbon data at 80°

Some early results obtained in September 1972 with a few minutes run are shown above in Figure 16. Four scatter plots are shown for two telescopes and two targets. The vertical axis in each case represents the energy loss in the thin counter, essentially dE/dx, and the horizontal is the energy loss in the thick counter, essentially the total energy for particles not crossing the second counter. Points accumulate mostly on the correct correlation curve for protons. Such curve folds back toward small energies when faster protons completely cross the second detector. Protons up to 32 MeV kinetic energy stop, while proton energies up to 100 MeV are measurable. Above the proton correlation curve points are seen to accumulate in two more bands which correspond to the correlation for deuterons and tritons. Also visible in Figure 16a and 16b are the increased density of points along the proton correlation curve corresponding to elastic P-P scattering from free H_2 in poly.

No such increase is observed in carbon.

The advantages of obtaining information on scattering on free protons by comparing scattering from polyethylene and carbon targets rather than using hydrogen targets are many: simplicity, high hydrogen density (0.14 mg/cm^2 as compared to $\sim$ 0.05 mg/cm^2 for liquid hydrogen and 10^{-3} mg/cm^2 for the hydrogen jet) and good geometry. The main problem in using such a method is in obtaining an accurate normalization of the data collected from poly and C in order to subtrack properly the carbon contribution from the poly data. Such normalization is obtained by counting deuterons and tritons produced in interactions with carbon nuclei in the polyethylene and carbon targets. Since these deuterons and tritons are detected simultaneously with the elastic events, we have a perfect method to obtain the product (effective beam intensity) x (number of carbon nuclei) in poly and C.[17]

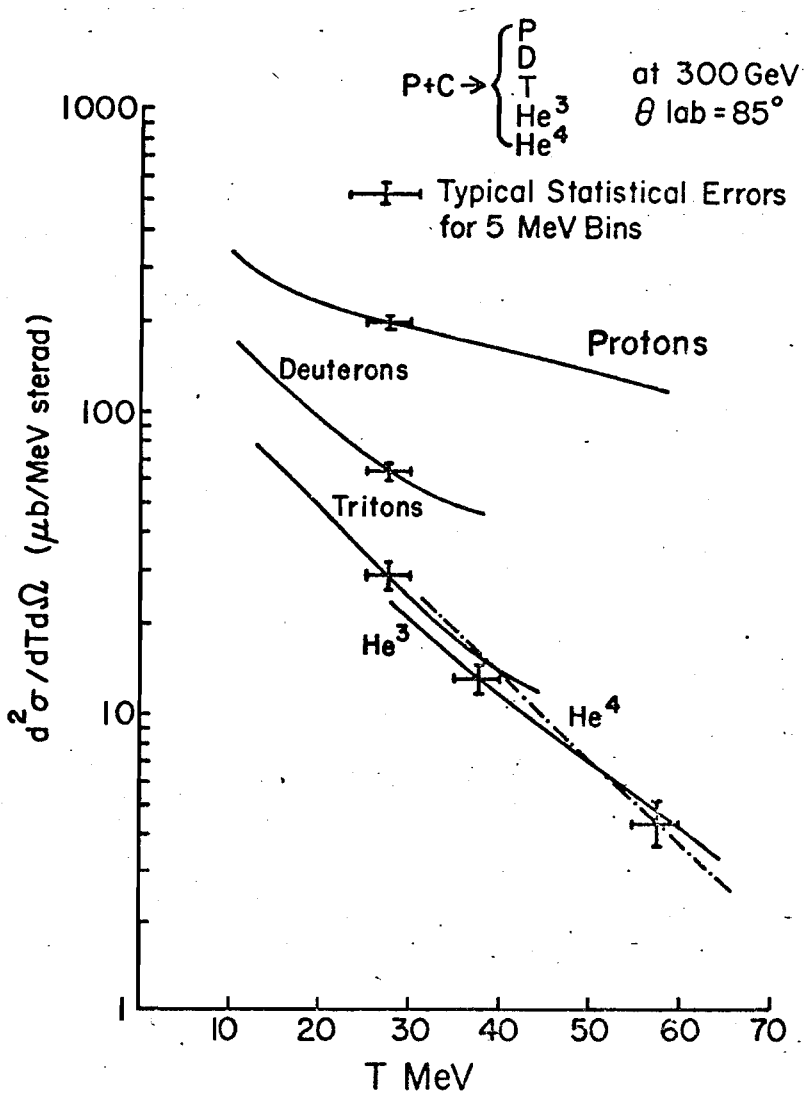

Figure 17. Doubly differential cross section versus kinetic energy for H^1, H^2, He^3, He^4.

Figure 17 gives the actual measured cross section for the emission of H^1, H^2, H^3, He^3 and He^4 at about 85° in the lab in 300 GeV proton-carbon interactions. A typical dE/dx - E plot illustrating the production of these fragments is shown in Figure 18.

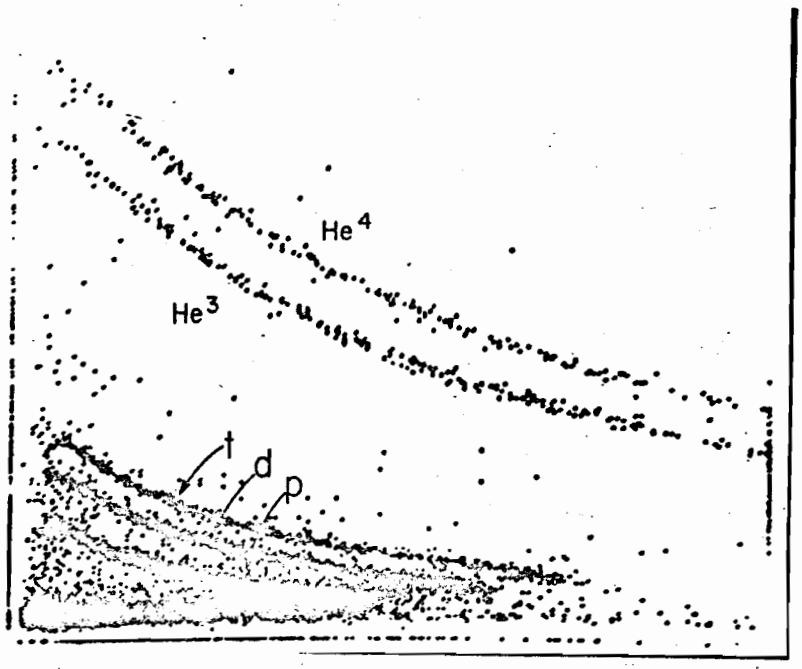

Figure 18. dE/dx - E plot showing particles observed in 300 GeV proton-carbon interactions.

The carbon subtraction can be performed with good statistical accuracy. In a one hour run we obtain typically 5×10^4 deuterons and tritons from both our polyethylene and carbon targets.

We perform the following steps to obtain the free hydrogen event distribution:

a) Divide the E_1, E_2 plane into a rectangular grid.
b) Count the number of deuterons and tritons from $(CH_2)_n$ and C.
c) Normalize the carbon event density from the C target to the one from $(CH_2)_n$ using b).
d) Subtract the normalized carbon event density from the $(CH_2)_n$ event density.

This procedure is carried out independently for each telescope. Then a deadtime correction is applied to each telescope. The next steps in the analysis are to obtain T from E_1 and E_2, and then from θ and T to compute M^2 and t as well as the Jacobian $\frac{\partial(\theta,T)}{\partial(t,M^2)}$. At this point $\frac{d^2N}{dtdM^2}$ is obtained in arbitrary units. The total number of inelastic scattering events on free hydrogen used for the above determination is approximately 110,000. An absolute normalization is

obtained from the total number of proton-proton elastic scattering events in each telescope which observes the elastic peak. 340,000 elastic scattering events were observed, the elastic peaks being clearly visible in seven telescopes. Such elastic peaks were also very useful to cross check our energy calibrations and our ability to correctly measure the t dependence of the cross section. To the accuracy of our data we obtain agreement with published values for the slope parameter.[18] We find $b = 10.7 \pm .6$, χ^2 of 18.9 for 19 degrees of freedom. See Figure 19.

Cp. 36
$b_0 = 8.23 \pm 0.28$

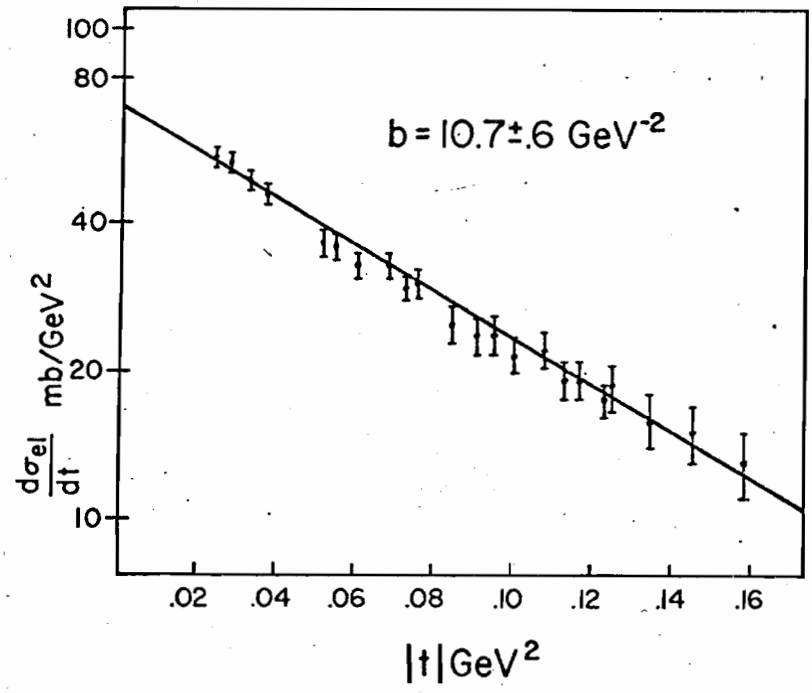

Figure 19. $\frac{d\sigma_{el}}{dt}$ versus $|t|$

The mass square resolution of this experiment was about 1 GeV^2, and can be seen directly in the following figure (Figure 20), where the spectrum is displayed including the elastic events. One notes that $\sigma = .55$ GeV^2.

The invariant cross section $\frac{s}{\pi} \frac{d^2\sigma}{dt dM_X^2}$ (s = total center of mass energy^2 = 563 GeV^2) versus M_X^2 for $|t|$ of .019 to .094 is seen in Fig-21. Also on the same graph is a plot of CHLM[7] data taken at $|t| = .35$ and S = 929.5, for comparison. One notes that our M_X^2 spectrum has a sharp peak at $M_X^2 = 2$ GeV^2 (it is the $N^*(1400)$), comes down steeply as M_X^2 increases, and has dropped to 1/20 of its peak value at $M_X^2 = 16$ GeV^2, thereafter the M_X^2 spectrum is approximately flat. This is in contrast with the ISR curve which has decreased only by a factor of five at a M_X^2 of 50 GeV^2. Note also that there the fall is gradual, approximately simulating $1/M_X^2$ dependence.

see $N^*(1400)$
ΔM @ 1400 $\approx$ 30 MeV

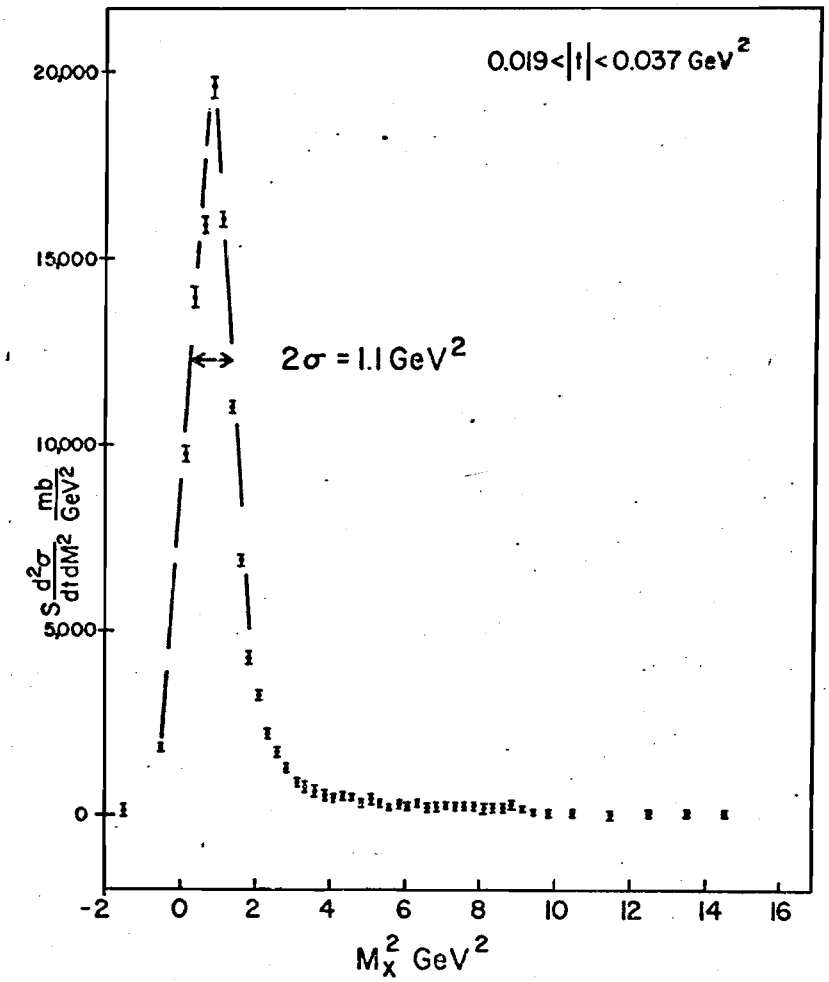

N*(1400) diffractively produced by Pomeron

Figure 20. $s \frac{d\sigma}{dt dM_X^2}$ versus M_X^2 for $.019 < |t| < .038$ $(GeV/c)^2$ including elastics.

The main question is whether the difference is due to the two experiments looking at two different regions $< |t| > = .056$ versus $< |t| > = .35$, or could be accounted for by resolution difference. We feel that it is primarily due to the latter since 1) the ISR curve has considerable area to the left of $M_X^2 = 0.0$, and 2) we have folded our curve with a resolution function of 10 GeV^2 and have obtained curves exceedingly similar to those of the ISR experiment (circled points), i.e. a depressed peak, slow fall off as M^2 increases, and having a higher cross section because it is at lower $< |t| >$. In conclusion, we feel the broadness of the ISR forward peak is due to their resolution, not because they are looking at a much higher $|t|$ region than we were. Therefore, we believe that the CHLM interpretation that there is substantial diffractive production of states with masses up to at least 7 GeV, is in

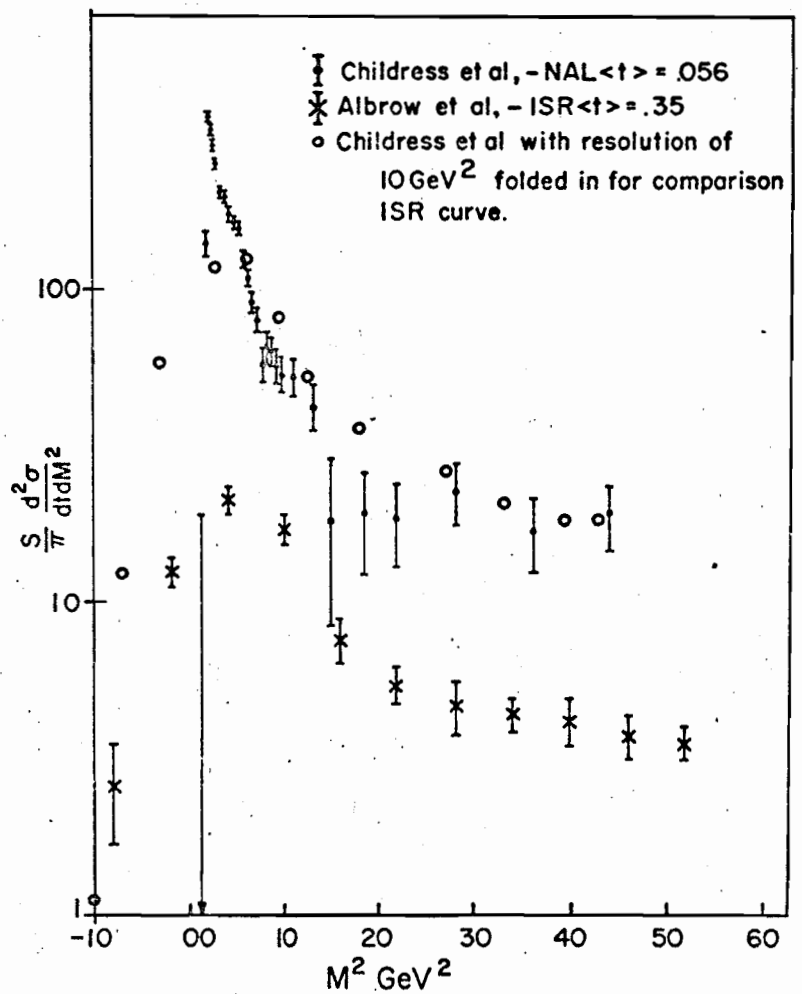

Figure 21. $\frac{s}{\pi}\frac{d^2\sigma}{dtdM_X^2}$ versus M_X^2 for $.019 < |t| < .094$ (GeV/c)^2 inelastic only

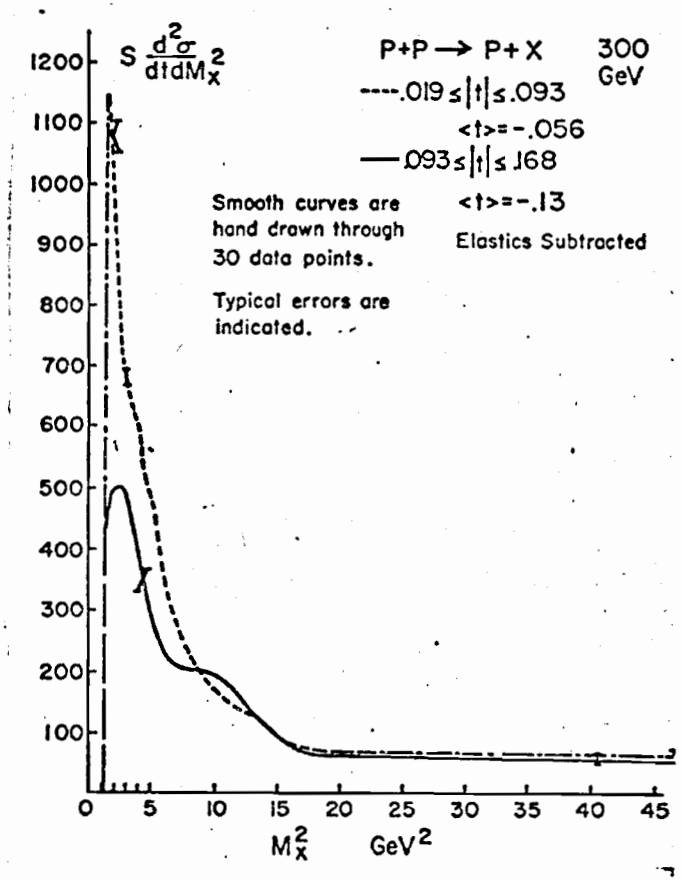

Figure 22. $s\frac{d^2\sigma}{dtdM_X^2}$ versus M_X^2 GeV^2 for <t> = -.056 and <t> = -.13.

disagreement with our experimental findings.

There are some differences in M_X^2 spectrum taken at different $|t|$ regions, but they are usually on details of structure. For example, we do not see the $N^*(1400)$ peak in our higher $|t|$ region data ($.09 < |t| < .17$), indicating a very sharp t dependence (slope b in e^{-bt} of the order of 18-20) for $N^*(1400)$ production.

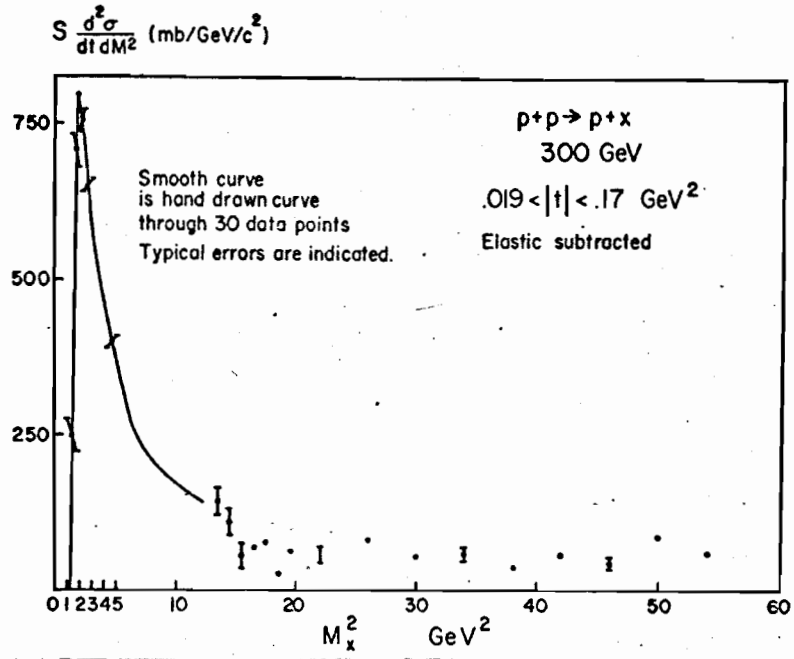

Figure 23. $s \frac{d^2\sigma}{dtdM_X^2}$ versus M_X^2 for $.019 < |t| < .19$ inelastic only

Figure 23 gives our determination of the inelastic invariant cross section $s \frac{d\sigma}{dtdM_X^2}$ for the whole t region of our experiment $.019 < |t| < .17$. We can estimate the total cross section from $1 < M_X^2 < 16\ \mathrm{GeV}^2$ to be $(2.35 \pm .2)$ mb using an average slope b of 4.3 determined from the same data. A lower bound for the diffraction contribution can be obtained by subtracting from this value the contribution due to whatever physical process is responsible for the essentially constant cross section above M_X^2 of 16 GeV^2. If this background is assumed to extend down to $M_X^2 = 1$ with the same value observed in the interval $16 \geq M^2 \geq 60\ \mathrm{GeV}^2$, we obtain

$$\sigma(PP \to PX,\ 1 \geq M_X^2 \geq 16\ \mathrm{GeV}^2,\ \text{diffractive?}) = 1.6 \pm .2\ \mathrm{mb}.$$

Multiplying this value by 2 for the symmetry of the PP system, we find the diffractive dissociation cross section is bounded by $3.2 \leq \sigma_{diff} \leq 4.7$ mb.

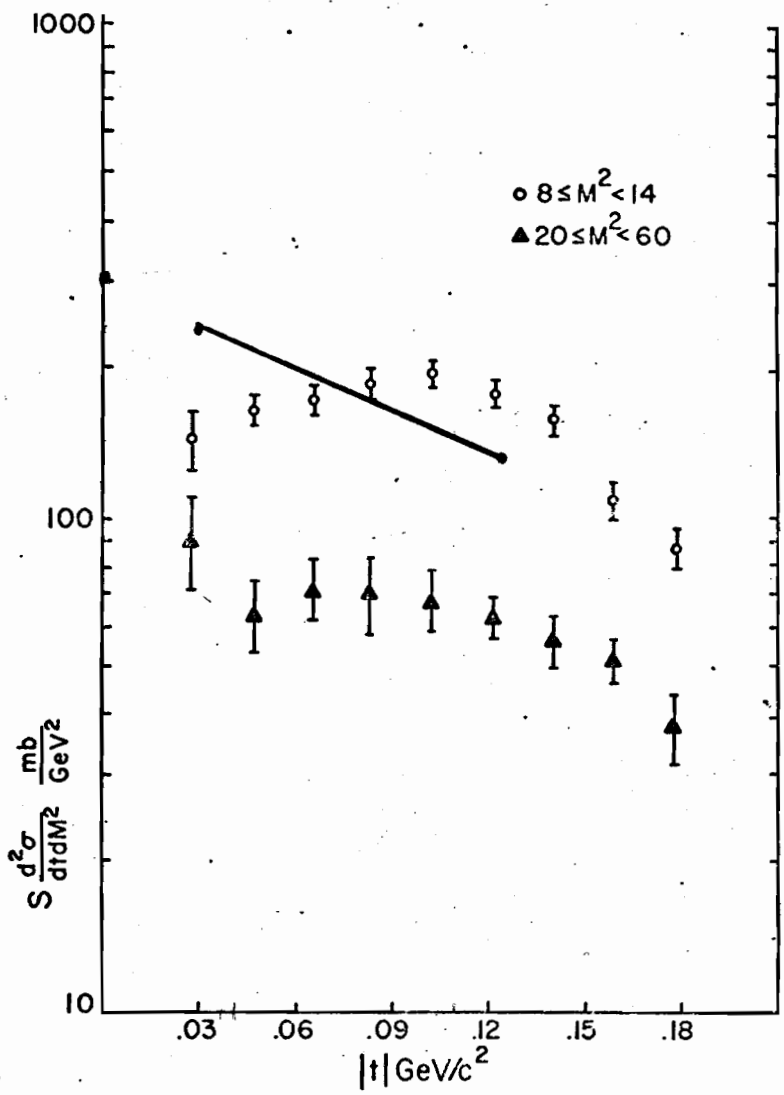

Figure 24. $s \frac{d^2\sigma}{dtdM_X^2}$ versus $|t|$ for $8\ \mathrm{GeV}^2 \leq M_X^2 \leq 14\ \mathrm{GeV}^2$, and $20\ \mathrm{GeV}^2 \leq M_X^2 \leq 60\ \mathrm{GeV}^2$.

Figure 24 shows a plot of the cross section versus $|t|$ for the mass square regions of $8\ \mathrm{GeV}^2 \leq M_X^2 \leq 14\ \mathrm{GeV}^2$, and $20\ \mathrm{GeV}^2 \leq M_X^2 \leq 60\ \mathrm{GeV}^2$. For the high M^2 region we can fit an exponential t dependence e^{-bt} with $b = 3.4 \pm 1.2$, $\chi^2 = 15$ for 7 degrees of freedom. The t dependence of the smaller M^2 region is clearly inconsistent with a single exponential. That the $|t|$ dependence should depend on M_X^2 can be readily seen by referring back to Figure 22, where we note the two spectra, one at $\langle t \rangle = -.056$ and the other at $\langle t \rangle = -.13$, cross each other twice at M_X^2 of $7\ \mathrm{GeV}^2$, $14\ \mathrm{GeV}^2$. The towering height of the lower $\langle t \rangle$ spectrum at $M^2 < 2\ \mathrm{GeV}^2$ relative to the higher $\langle t \rangle$ region is what yields the high b value of 15-18 for the N^* production.

One sees a reversal of the relative height of the two spectra in the region $7 < M_X^2 < 14$ GeV^2, and the approximate coincidence of the two spectra until 17 GeV^2. From 17 GeV^2 on the $\langle t \rangle = -.13$ spectrum remains lower than the $\langle t \rangle = -.056$ spectrum. This intriguing connection between the $|t|$ dependence and the M_X^2 will be investigated in detail in our coming experiment in the Internal Target Area at NAL.[19]

When extrapolated to the $|t|$ regions measured by ISR and Rutgers, our cross sections are consistent with theirs. See Figure 25.

Consistent with Exp #188

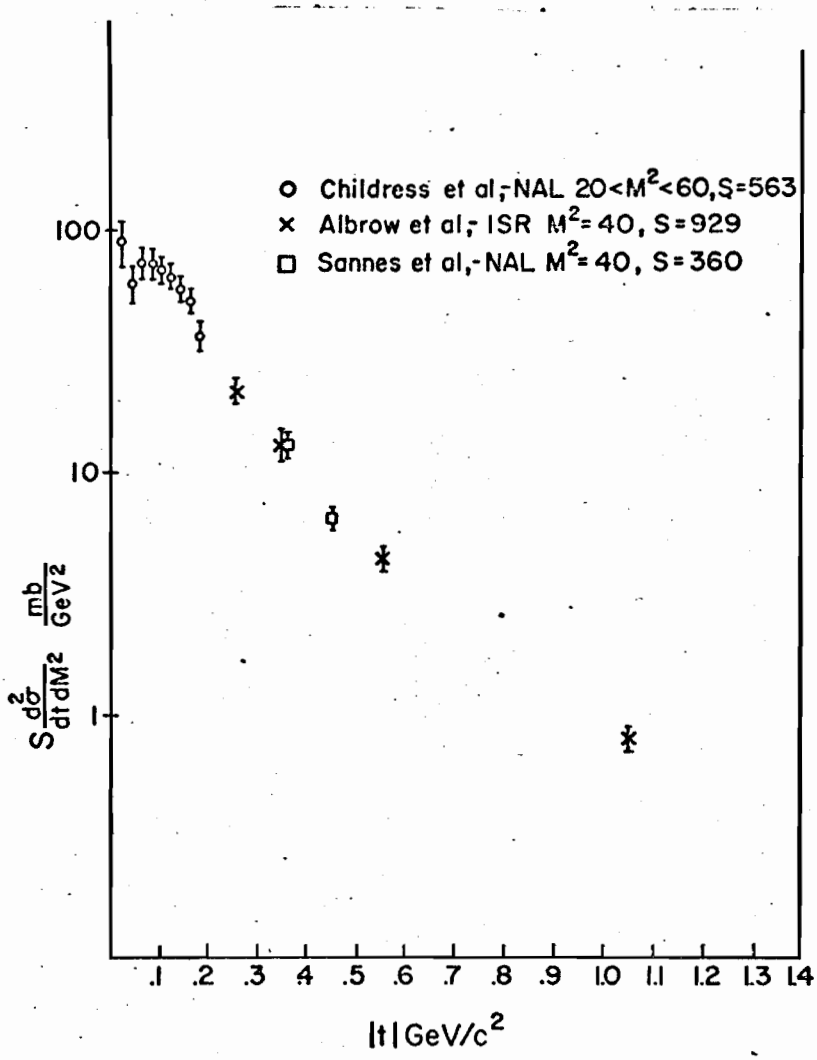

Figure 25. $s \frac{d^2\sigma}{dt dM_X^2}$ versus $|t|$ for this experiment, ISR, and Rutgers

SUMMARY

The results of the aforementioned experiments can be summarized by the following graph (Figure 26). We note that different parts of the M_X^2 spectrum have their own distinct t and s dependences. The associated multiplicities are also M_X^2 dependent. Quantatively, if one assumes the scaling part of the cross section extends to $M_X^2 = 1$, then the diffractive dissociation cross section is of the order $1.6 \times 2 \simeq 3.2$ millibarns.

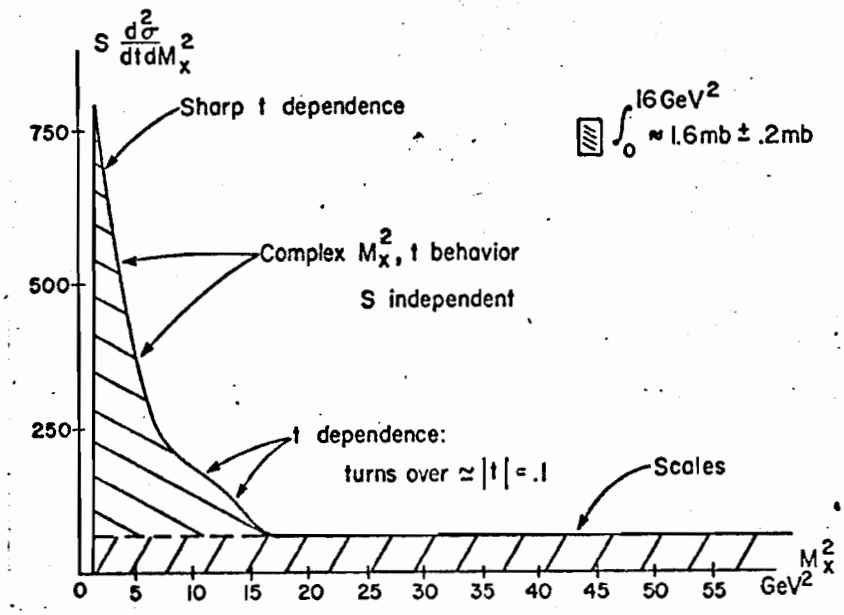

Figure 26. $s \frac{d^2\sigma}{dtdM_X^2}$ versus M_X^2

FITTING OF DATA

A. Polynomial Fit

Can the behavior of the M_X^2 spectrum be adequately described by a few term polynomial in $1/M_X$? The rapoteur for the CHLM experiment, as well as several NAL bubble chamber experiments, have reported at the Berkeley Conference in the affirmative.[11] The high resolution data in Figure 23 cannot be characterized by just a $1/M_X^2$ dependence because of its fast decrease with increasing M_X^2. In Figure 27 an attempt to fit that spectrum with the combination of a $1/M_X^2$ and a constant term is shown by the dashed curve. One obtains

$$s \frac{d^2\sigma}{dtdM_X^2} = s \left[2.75 \left(\frac{1}{M_X^2}\right) + .036 \right] \frac{mb}{GeV^2}$$

where $s = 563\ GeV^2$. One notes that most of the data points in the

steeply falling region miss this dashed curve by more than six standard deviations, hardly an acceptable fit. The solid curve is the combination of a $1/M_X^3$ dependence and a constant term, and one obtains:

$$s \frac{d^2\sigma}{dtdM_X^2} = s \left[6\left(\frac{1}{M_X^3}\right) + .089 \right] \frac{mb}{GeV^2}$$

Note that the steeply falling region is fitted much better by a $1/M_X^3$ dependence. Clearly both $1/M_X^2$ and $1/M_X^3$ terms are necessary.

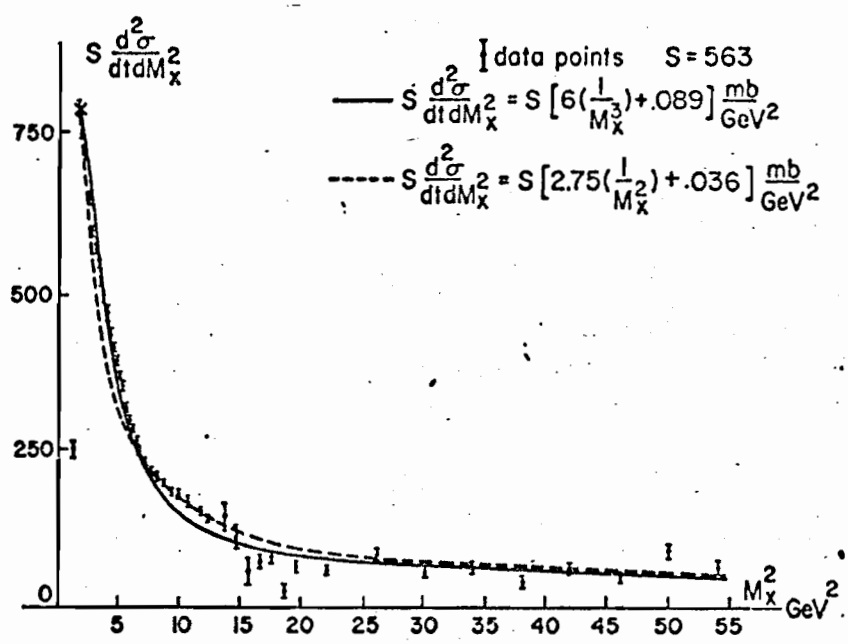

Figure 27. Polynomial fit of $s \frac{d^2\sigma}{dtdM_X^2}$ versus M_X^2 GeV^2

B. Triple Regge Fit.

A. Mueller[20] has generalized the optical theorem from which one relates the total cross section in 2-body scattering with the imaginary part of the forward elastic amplitude ($ab \to ab$) to one which relates the inclusive cross section ($ab \to cX$) to a particular discontinuity of the forward amplitude of the elastic 3-body process ($ab\bar{c} \to ab\bar{c}$). But what is the forward elastic 3-body amplitude? Some theorists[5] have expanded the 3-body elastic amplitude in terms of Regge Poles in various regions of asymptopia. In particular, where $M_X^2 \to \infty$, $s \to \infty$, and s/M_X^2 and t are held fixed, they write

$$s \frac{d^2\sigma}{dtdM_X^2} = \frac{\sum_{ijk}}{s} \gamma^i_{b\bar{c}}(t)\, \gamma^j_{b\bar{c}}(t)\, \gamma^k_{a\bar{a}}(t) \cdot \Gamma_{ijk}(t) \left(\frac{s}{M_X^2}\right)^{\alpha i(t)+\alpha j(t)} \left(M_X^2\right)^{\alpha_k(0)}$$

where the γ's are reggeon-particle coupling constants and Γ_{ijk} is a triple regge vertex describing the coupling of three reggeons $\alpha_i(t)$, $\alpha_j(t)$, $\alpha_k(0)$. Pictorially, this is seen in Figure 28.

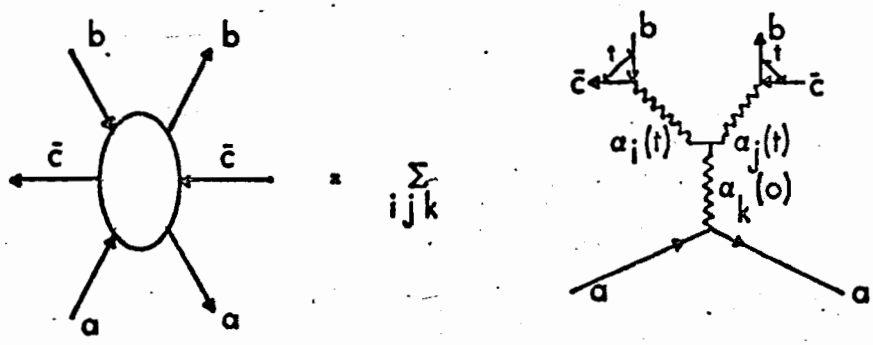

Figure 28. Diagram for two-particle inclusive reaction

It is also assumed that the leading singularity exchanged in the $a\bar{a}$ channel is the Pomeron with intercept 1 and the next to leading singularities are the meson trajectories f, ρ, ω and A_2 with intercept 1/2. Furthermore, the f and ω are preferred over ρ and A_2.[22] Finally, the paucity of data in the past has made it customary to drop all interference terms and fit the M_X^2 spectrum with just two or three terms.[23] An amusing aside is that in this wonderland $M_X^2 \to \infty$, $s \to \infty$ can be approximated by $M_X^2 > 4$ GeV^2 and $s \simeq 80$ GeV^2. In short, despite great personal reservations, we write approximately:

$$s\,\frac{d^2\sigma}{dt\,dM_X^2} = \frac{1}{s}\left[G_{PPP}(t)\left(\frac{s}{M_X^2}\right)^{\alpha_p(t)+\alpha_p(t)}(M_X^2)^{\alpha_p(0)}\right.$$

$$\left. + G_{PPR}(t)\left(\frac{s}{M_X^2}\right)^{\alpha_p(t)+\alpha_p(t)}(M_X^2)^{\alpha_R(0)} + G_{RRP}(t)\left(\frac{s}{M_X^2}\right)^{\alpha_R(t)+\alpha_R(t)}(M_X^2)^{\alpha_P(0)}\right]$$

where $\alpha_P = 1 + .28t$ (the value .28 taken from the recent U.S.-U.S.S.R. determination), and $\alpha_R = .5 + t$. Note that at small t, for constant s, the triple pomeron term essentially gives a $1/M_X^2$ dependence of the M_X^2 spectrum, the pomeron-pomeron-reggeon term gives a $1/M_X^3$ dependence , and the reggeon-reggeon-pomeron term gives essentially a constant term in the M_X^2 spectrum.

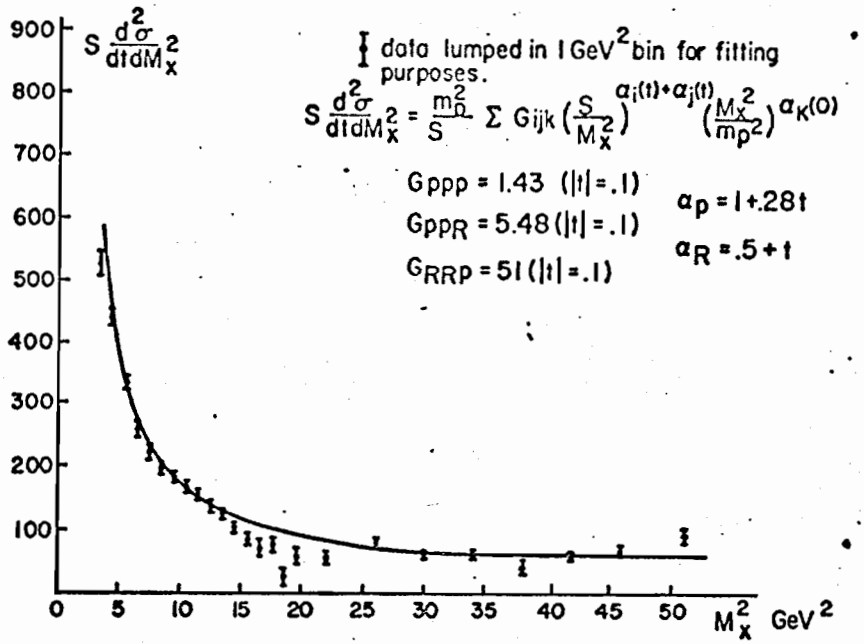

Figure 29. Triple Regge fit of $s \frac{d^2\sigma}{dtdM_X^2} \frac{mb}{GeV^2}$ versus M_X^2 GeV^2

Figure 29 shows our best fit, yielding the following values:

$G_{PPP} = 1.43$ (mb/GeV^2) at ($t = -.1$)
$G_{PPR} = 5.48$ (mb/GeV^2) at ($t = -.1$)
$G_{RRP} = 51$ (mb/GeV^2) at ($t = -.1$)

which taken simply, restates that the $1/M_X^3$ dependence is important for describing the behavior of data. It is also clear that this parameterization being the simple superposition of three terms of a polynomial, could never reproduce interesting structures seen in the data, for example, in the neighborhood $7 < M_X^2 < 14$ GeV^2 and $15 < M_X^2 < 22$ GeV^2.

Gerson Goldhaber[8] had made a fit with the ACGHT data, taking into account the rather wide M_X^2 resolution, to extract the dominant triple regge coupling. He obtained a value of $\nu = 1.15 \pm 0.1$, where a ν of 1 would correspond to triple pomeron dominance and a ν of 3/2 would correspond to PPR dominance.

CONCLUSION

p-p inelastic scattering at small momentum transfer proves itself to be a rather complex phenomenon. Especially puzzling are the interlocking M_X^2, s and t dependences. In order to separate out the various mechanisms, it is imperative to have systematic data with

fine resolution, high statistics, covering a wide range in s, t, and M_X^2. Our (CFL-FMS) next experiment[19], using the apparatus described in Section E, will be located at the Internal Target Area of the National Accelerator Laboratory. With the automatic s variation of the proton beam from the acceleration cycle available to us, we hope to perform a series of measurements which will have the aforementioned desirable characteristics within the year.

REFERENCES

1. E.W. Anderson, et al., Phys. Rev. Letters 19, 198 (1967),
   R.M. Edelstein, et al., Phys. Rev. D5, 1073 (1972),
   J.V. Allaby, et al. Nucl. Phys. B52, 316 (1973).
2. M.L. Good and W.D. Walker, Phys. Rev. 120, 1857 (1960).
3. R.K. Adair, Phys. Rev. 172, 1370 (1968),
   M. Jacob and R. Slansky, Phys. Letters 37B, 408 (1971),
   K. Gottfried and O. Kofoed-Hansen, Phys. Letters 41B, 195 (1972).
4. G.O. Freund, Phys. Rev. Letters 21, 1375 (1968).
5. O. Kancheli, Pisma Zh. Eksp. Teor Fiz 11, 397 (1970)
   [JETPLetters 11, 267 (1970)]
   R.D. Peccei and A. Pignotti, Phys. Rev. Letters 26, 1076 (1971),
   C.E. DeTar, et al., Phys. Rev. Letters 26, 675 (1971),
   H.D.Z. Abarbanel, et al., Phys. Rev. Letters 26, 937 (1971).
6. R.P. Feynman, Phys. Rev. Letters 23, 1415 (1969), and private communication.
7. M.G. Albrow et al., Nucl.Phys. B54, 6 (1973),
   M.G. Albrow, et al., Nucl. Phys. B51, 388 (1973).
8. ACGHT Collaboration, quoted in M. Jacob, CERN Pre-Print TH-1683 (Lectures given at the CERN-JINK School).
9. R. Cool, et al., Contribution to the 1973 Meeting of the APS Division of Particles and Fields, Berkeley, August 13-17, 1973.
10. F. Sannes, et al., Contribution to the 1973 Meeting of the APS Division of Particles and Fields, Berkeley, August 13-17, 1973.
11. J. Van de Velde, Contribution to the Fifth International Conference on High Energy Collisions, Stony Brook, August23-24, 1973.
12. M.G. Albrow, et al., Phys. Letters 44B, 207 (1972).
13. R. Schamberger, et al., Contribution to the 1973 Meeting of the APS Division of Particles and Fields, Berkeley, August 13-17, 1973,
    S. Childress, et al., Contribution to the Meeting of the APS Division of Particles and Fields, Berkeley, August 13-17, 1973.
14. R. McCarthy, et al., Experiments on High Energy Particle Collisions-1973, (Vanderbilt Conference).
15. P. Franzini and R. Schamberger, Contribution to the 1973 International Conference on High Energy Collisions, Frascati, Italy.
16. P. Franzini, et al., Contribution to the 1973 International Conference on High Energy Instrumentation, Frascati, Italy.
17. J. Lee-Franzini, et al., Contribution to the 1973 Internationsl Conference on High Energy Instrumentation.
18. Barbiellini et al., Phys. Letters 39B, 663 (1972).
19. Experiment 221, NAL.
20. A.H. Mueller, Phys. Rev. D2, 2963 (1970).
21. J. Lee-Franzini, to be published in the Proceedings of the 1973 Meeting of the APS Division of Particles and Fields, Berkeley.
22. G.V. Dass and C. Michael, Phys. Rev. Letters 20, 1066 (1968).
23. S.D. Ellis and A.Z. Sanda, Phys. Rev. D6, 1347 (1972).
    F.E. Paige and L.L. Wang, Nucl. Phys. B46, 477 (1972).